Post-print of: Journal of Sol-Gel Science and Technology, volume 86, 2018, Pages 316–328

Kinetics of the acid-catalyzed hydrolysis of tetraethoxysilane (TEOS) by ^{29}Si NMR spectroscopy and mathematical modelling

J.C. Echeverría[1,2 *], P. Moriones[1,2], G. Arzamendi[1,2], J.J. Garrido[1,2], M.J. Gil[1,2], A. Cornejo[1,2], V. Martínez-Merino[1,2]

[1] *Departamento de Química Aplicada, Edif. Los Acebos, Universidad Pública de Navarra, Campus Arrosadía, 31006 Pamplona, Spain.*

[2] *Institute for Advanced Materials, Edif. Jerónimo de Ayanz, Universidad Pública de Navarra, Campus Arrosadía, 31006 Pamplona, Spain.*

** Corresponding author.*

E-mail address: jesus.echeverria@unavarra.es

Phone number: (34) 948168967

ORCID numbers:

J. Echeverría: //orcid.org/0000-0001-8126-1429

P. Moriones://orcid.org/0000-0002-9340-7728

G. Arzamendi: //orcid.org/0000-0002-6276-8029

J.J. Garrido: //orcid.org/0000-0002-3366-9726

M.J. Gil: //orcid.org/0000-0001-6174-7309

A. Cornejo: //orcid.org/0000-0001-8810-0062

V. Martínez-Merino: //orcid.org/0000-0002-1873-0699

Keywords

Mathematical modelling, kinetic constants, TEOS, ^{29}Si NMR, pH-independent rate constants, activation energy

Highlights

- Hydrolysis reactions had a common pathway, independent of pH and temperature.
- The system is described with six kinetic constants, six activation energies and the equilibrium constant for the forth hydrolysis
- The activation energy for condensation from $Si(OH)_4$ to form ≡Si─O─Si≡ was ca. 10 kJ mol^{-1} higher than the largest activation energy in the hydrolytic reactions.
- The pH-independent rate constants at 298.2 K increased as the hydrolysis progresses.

Abstract

Tetraethoxysilane (TEOS) is widely used to synthesize siliceous material by the sol-gel process. However, there is still some disagreement about the nature of the limiting step in the hydrolysis and condensation reactions. The goals of this research were to measure the variation in the concentration of intermediates formed in the acid-catalyzed hydrolysis by ^{29}Si NMR spectroscopy, to model the reactions, and to obtain the rate constants and the activation energy for the hydrolysis and early condensation steps. We studied the kinetics of TEOS between pH 3.8 and 4.4, and four temperature values in the range 277.2 – 313.2 K, with a TEOS:ethanol:water molar ratio 1:30:20. Both hydrolysis and condensation rate speeded up with the temperature and the concentration of oxonium ions. The kinetic constants for hydrolysis reactions increased in each step $k_{h1} < k_{h2} < k_{h3} < k_{h4}$, but the condensation rate was lower for dimer formation than for the formation of the fully hydrolyzed $Si(OH)_4$. The system was described according to thirteen parameters: six of them for the kinetic constants estimated at 298.2 K, six to the activation energies, and one to the equilibrium constant for the fourth hydrolysis. The mathematical model shows a steady increase in the activation energy from 34.5 kJ mol^{-1} for the first hydrolysis to 39.2 kJ mol^{-1} in the last step. The activation energy for condensation reaction from $Si(OH)_4$ was ca. 10 kJ mol^{-1} higher than the largest activation energy in the hydrolytic reactions. The decrease in the net positive charge on the Si atom contributes to the protonation of the ethoxy group and makes it a better leaving group.

1 Introduction

The preparation of siliceous materials by the sol-gel process is widely used for coatings, adsorbents, catalyst supports, fiber optic sensors, photovoltaic devices, cosmetics and drug delivery [1]. The synthesis of siliceous materials by the sol-gel process includes hydrolysis reactions of precursors, condensation of hydrolyzed species to form colloidal suspensions, and reactions between colloids to form a gel network of silica with the solvent embedding the pores. Because of the huge number of parameters to be controlled, the sol-gel process is very versatile and, therefore, the chemical properties and porous texture of xerogels can be controlled by tuning the pH, temperature, and the molar ratio of the precursor, water and solvent [2-7].

Although the sol-gel process has been widely studied, the nature of the limiting step in the hydrolysis and condensation reactions remains controversial. In spite of the efforts made by numerous authors who have investigated the hydrolysis and condensation reactions when tetraethylorthosilicate (TEOS) is used as silicon precursor to prepare xerogels, rationalization for kinetic trends and kinetic mechanisms is still under discussion. In particular, several authors have reported that each subsequent hydrolysis from TEOS to $Si(OH)_4$ is slower than the precedent [2,8]. However, this trend is the opposite of the experimental results reported by other authors [9-11]. This discrepancy in the kinetic trends from experimental results limits the understanding of the overall mechanism for the polymerization process, which depends on the type and concentration of oligomers [12].

A comparison of experimental rate constants is also restricted by the different reaction conditions. Most authors set the reported pH of the reaction by using acidified water and hence the concentration of oxonium ions is that of water, which is different from the actual pH and $[H_3O^+]$ at the reaction medium [13]. Additionally, most of the reported experiments have been directly performed in the NMR tubes which reduces sample manipulation.

^{29}Si NMR is the most commonly used technique to identify the different Si containing species produced in sol-gel processes [14-16]. This spectroscopic technique is a very powerful tool which can distinguish silicon atoms attached to different combinations of ligands. In addition, ^{29}Si NMR can quantitatively monitor Si sites with

different connectivity and, therefore, determine concentration of the hydrolysis intermediates and the beginning of condensation reactions, including small oligomers present in the system, and show whether these oligomers are cyclic, linear, or branched.

Unfortunately, the high specificity of this technique is not equaled by its sensitivity. The low natural abundance of ^{29}Si, its low gyromagnetic ratio, and the rather long relaxation times limit the application of ^{29}Si NMR spectroscopy for following fast hydrolysis and condensation reactions in real time [14,17]. However, the low sensitivity can be circumvented by accumulating more pulses and by adding paramagnetic transition metal complexes such as chromium acetylacetonate ($Cr(acac)_3$) to reduce the relaxation time [18-20]. The data collection time for a reasonable signal-to-noise ratio in ^{29}Si NMR spectroscopy depends on the concentration of the silicon species and the mobility of these species, since condensed phases produce weaker signals [13].

The goal of this research was to investigate the kinetics in the acid-catalyzed hydrolysis of TEOS as a function of pH and reaction temperatures. The specific goals were the following: (a) to measure the variation in concentration of the structural intermediates formed during hydrolysis and early condensation reactions in TEOS sol-gel by ^{29}Si NMR spectroscopy, (b) to fit the quantitative kinetic data to model the reactions, (c) to obtain the rate constants for the hydrolysis and initial condensation reactions, and (d) to obtain the activation energy for the hydrolysis and condensation processes.

2 Materials and methods

2.1 Preparation of samples

The molar concentrations for the studied samples were as follows: 0.426 mol L^{-1} TEOS, 12.80 mol L^{-1} ethanol and 8.53 mol L^{-1} water, which results in a molar ratio precursor: ethanol: water of 1:30:20. The ethanol concentration was high enough to make sure the miscibility of the reagents mixture. While continuously stirring with a magnetic bar, 1.505 mL of TEOS (purity ≥ 98%, Sigma Aldrich, Steinheim, Germany) as a silica precursor and 11.605 mL of absolute ethanol as a solvent (GR for analysis, Sigma Aldrich Chromasolv®, Steinheim, Germany) were mixed in a 30 mL glass container with a diameter of 35 mm and screw cap (Scharlab, Barcelona, Spain). Then, a pre-established volume of water (Mili-Q grade) was added dropwise under magnetic

stirring. The pH of the solution was adjusted to pH 3.8, 4.1 or 4.4 by adding 0.05 mol L^{-1} HCl (Merck, Darmstadt, Germany) with an automatic burette (Titrino mod. 702 SM, Metrohm, Herisau, Switzerland). The amount of water was set at a total volume 2.385 mL. Finally, the containers with solutions were closed and left in an oven (HOTCOLD-A 2101502, JP Selecta, Barcelona, Spain, ± 0.1 K) without magnetic stirring, at different temperatures (277.2, 283.2, 293.2, 313.2 K).

2.2 Spectra collection and silicon species quantification

We chose to measure the kinetics in a set of experimental conditions as similar as possible to those used in the synthesis of the material instead of monitoring the hydrolysis process in an NMR tube. Furthermore, chromium salt was only added upon measuring the NMR spectra to prevent any variation in reaction kinetics. Similarly, deuterated solvent was added in the minimal amount to lock the NMR spectrometer signal while keeping sample homogeneity. At pre-established reaction times, NMR samples were prepared in 5 mm OD tubes by mixing 400 µL of reaction solution with 100 µL of 0.104 mol L^{-1} $Cr(acac)_3$ in deuterated dimethylsulfoxide, DMSO-d_6 (Carlo-Erba).

^{29}Si NMR spectra of samples were recorded on a 400 MHz Bruker Advance III (4.1 T) spectrometer equipped with a 5 mm Pabbo probe. The frequency for ^{29}Si was tuned at 79.486 MHz and the frequency for ^{1}H was tuned at 400.132 MHz. ^{1}H was measured using the preinstalled *zg30* program without any modification. The pre-installed pulse program *zgig* parameters were modified for ^{29}Si analysis; the d1 delay was set to 0 s and the length of p1 was 4.00 µs with simultaneous irradiation of ^{1}H nuclei at 0.2663 W (PLW=12) for 80 µs thus preventing Si-H coupling. The mixture was vigorously stirred before analysis. NMR tubes were spun at a frequency of 20 Hz. Measurements were done under isothermal conditions at 300 K.

The signals corresponding to the hydrolyzed species were well resolved under the experimental conditions. ^{29}Si signal corresponding to the hydrolyzed species from TEOS were assigned according to the literature [2,10,21]. Calibration of the ^{29}Si signal against TEOS concentration was done using samples of known concentration of TEOS. Linear regression analyses between the intensity of the ^{29}Si signal and the concentration of TEOS were performed using the data analysis software MS-Excel® to obtain the

calibration curve and the standard error of the slope and the origin ordinate. When no condensation products were present in the sample, the sum of the intensity of the TEOS and the hydrolyzed species was equal to initial intensity for the signal of TEOS within the random error of the measurement and we assumed that the concentration of each hydrolyzed species was proportional to the concentration. The relative concentration for TEOS and intermediate hydrolysis species was thus determined by measuring the absolute intensity of the corresponding signals in the spectra.

2.3 Mathematical modelling of kinetics

In view of the available information in the literature, and based on our own experimental results, a kinetic model has been developed in this work. The global process is made up by hydrolysis reactions followed by condensation reactions (Eq. (1) – (6)). Four consecutive stages of hydrolysis have been taken into account, and in each hydrolysis step a molecule of ethanol (EtOH) is produced. The fourth hydrolysis reaction is reversible according to Fyfe et al. [10,22]. Finally, the condensation reactions between the silanol groups of $Si(OH)_4$ and between the silanol groups of $Si(OH)_4$ and the free silanol groups in condensed species have been considered. We checked other condensation reactions involving silanol groups of hydrolysis intermediates without any improvements in the adjusted parameters.

Hydrolysis

$$Si(OC_2H_5)_4 + H_2O \xrightarrow{k_{h1},[H_3O^+]} Si(OC_2H_5)_3(OH) + C_2H_5OH \quad (1)$$

$$Si(OC_2H_5)_3(OH) + H_2O \xrightarrow{k_{h2},[H_3O^+]} Si(OC_2H_5)_2(OH)_2 + C_2H_5OH \quad (2)$$

$$Si(OC_2H_5)_2(OH)_2 + H_2O \xrightarrow{k_{h3},[H_3O^+]} Si(OC_2H_5)(OH)_3 + C_2H_5OH \quad (3)$$

$$Si(OC_2H_5)(OH)_3 + H_2O \underset{k_{-h4},[H_3O^+]}{\overset{k_{h4},[H_3O^+]}{\rightleftharpoons}} Si(OH)_4 + C_2H_5OH \quad (4)$$

Condensation

$$2\ Si(OH)_4 \xrightarrow{k_{c1},[H_3O^+]} (OH)_3Si\text{-}O\text{-}Si(OH)_3 + H_2O \quad (5)$$

$$(OH)(Si(OR)_2O)_n\text{-}Si(OH)_3 + Si(OH)_4 \xrightarrow{k_{c2},[H_3O^+]} (OH)(Si(OR)_2O)_{n+1}\text{-}Si(OH)_3 + H_2O \quad (6)$$

The kinetic model has been developed on the basis of the following premises: (a) the reacting system is homogeneous so the concentrations of all the chemical compounds refer to the total volume of the reaction mixture; (b) all reactions are assumed elementary. Under these premises, mass balances for the several chemical compounds (i), can be deduced from the following general expression:

$$\frac{dC_i}{dt} = \sum_j \nu_{ij} \cdot R_{ij} \tag{7}$$

where, ν_{ij} is the stoichiometric coefficient of species i in reaction j, which is considered to be negative for the reactants and positive for the reaction products; R_{ij} is the reaction rate for species i in reaction j. The general expression in Eq. 7 is specified for each species in supplementary material file.

Equations of concentration derivatives were integrated by a Fortran Compiler that includes the IMSL subroutines library. The ordinary differential equations were solved using the DIVPRK subroutine that applies the 5th and 6th orders adaptive Runge–Kutta–Verner method. Additionally, the reaction rate data were fitted by means of nonlinear regression analysis using the Nelder and Mead algorithm of direct search furnished by the DBCPOL subroutine in the IMSL library. An objective function (F) given by the sum of the relative differences between the experimental concentration of the evaluated species and the values predicted by the kinetic model was established.

$$F = \sum_t \frac{1}{N_r} \sum_t \sum_i^s \left(C_i^{exp}(t,r) - C_i^{mod}(t,r) \right)^2 \tag{8}$$

where $C_i^{exp}(t,r)$ and $C_i^{mod}(t,r)$ are the experimental and model calculated values of the concentration of component *i* in the instant *t* in the experimental run, *r*; and N_r being the number of experimental observations in each run *r*. The species evaluated were TEOS, $Si(OC_2H_5)_3(OH)$, $Si(OC_2H_5)_2(OH)_2$, $Si(OC_2H_5)(OH)_3$, and $Si(OH)_4$.

Additionally, if the water concentration is assumed to be constant, the concentration of TEOS, $C_{TEOS}(t)$, and the first hydrolysis, $C_{Si(OEt)3(OH)}(t)$, can be obtained upon integration of their corresponding balances [23].

$$C_{TEOS}(t) = C_{TEOS,0} \cdot e^{-k'_{h1} C_{H_2O,0} \cdot t} \quad (9)$$

$$C_{Si(OC_2H_5)_3(OH)}(t) = C_{TEOS,0} \cdot \frac{k'_{h1}}{k'_{h2} - k'_{h1}} \left(e^{-k'_{h1} C_{H_2O,0} \cdot t} - e^{-k'_{h2} C_{H_2O,0} \cdot t} \right) \quad (10)$$

where $C_{TEOS,0}$ and $C_{H2O,0}$ are the initial concentrations of TEOS and water, respectively; k'_{h1} and k'_{h2} are the kinetic constants for the first and second hydrolysis steps. These data have been fitted by means of nonlinear regression analysis using a modified Levenberg-Marquardt method furnished by the DRNLIN subroutine in the IMSL library.

2.4 Quantum Mechanic Calculations

All calculations in this work were performed with the Gaussian 09 program suite [24]. Full geometry optimizations and analytical vibrational frequency calculations have been performed for all compounds at the mPW1PW91level of theory using the standard 6-31G(d) basis set for the main group elements [25]. Stationary points were characterized by exactly zero imaginary vibrations respectively. Attached proton test (APT) atomic charges were calculated at the same level of theory [26]. Natural Population Analyses (NPA) [27] were also performed on all compounds at B3LYP level, using 6-311+G(2d,p) basis set for the main group elements that includes splits, diffuse and polarization functions, in order to obtain atomic natural charges [28,29]. NMR shielding tensors were computed with the and the Gauge-Independent Atomic Orbital (GIAO) method at B3LYP/6-311+G(2d,p) level of theory on mPW1PW91/6-31G(d) geometries in gas phase [30-32].

3 Results

The TEOS: EtOH: H_2O ratio was chosen to ensure homogeneity of the sample as well as to ensure that the amount of water is in excess. The pH range 3.8 – 4.4 was chosen for convenience; if the pH is lower than 3.8 and the temperature is equal or higher than 293.2 K, the reaction rate is too fast to be monitored by ^{29}Si NMR. On the other hand, if the pH is higher than 4.4 and the temperature is equal or lower than 277.2 K the reaction kinetics is too slow to have practical interest. Finally, the pH was adjusted in the reacting samples instead of using acidified water. Given the precision and rapidity of the automatic burette, the lapse of time for the pH setting was lower than

the time required to achieve a ^{29}Si NMR spectra, which varied between 12 and 15 min. The experimental spectra are indeed an average of the sample during this time. Regarding the quantification of the silicon species, we first considered using internal standards. Among others, tetramethylsilane, tetraethylsilane or 3-(trimethylsilyl)-1-propanesulfonic acid sodium salt were tested but, either because of the low solubility or the partial evaporation of the internal standard, the results were not reliable. Direct calibration of the ^{29}Si absolute intensity (I) against TEOS concentration in the sample was a suitable methodology to monitor the hydrolysis process as is shown by the low dispersion of the experimental results. Furthermore, as hydrolysis goes by, the sum of the intensity of all monomeric Si species in the solution corresponded to the starting signal of TEOS, enabling both a normalization of the response and an estimation of condensation products by using a mass balance.

3.1 ^{29}Si NMR spectra

Fig. 1 shows typical ^{29}Si NMR spectra during the hydrolysis of TEOS and condensation of hydrolyzed species at pH 4.1 and 293.2 K. Under these experimental conditions, the peaks of the hydrolyzed species are well resolved. The peaks were assigned to corresponding silicon atoms according to the literature [2,10,13,33]: the TEOS signal appeared at – 82.1 ppm, $Si(OC_2H_5)_3(OH)$ at – 79.1 ppm, $Si(OC_2H_5)_2(OH)_2$ at – 76.7 ppm, $Si(OC_2H_5)(OH)_3$ at – 74.7 ppm, and $Si(OH)_4$ at – 72.8 ppm. Condensation products are not as well-resolved, the dimer peaks appeared between – 82.1 and – 82.3 ppm, being the most noticeable signal at – 82.1 ppm. Si atoms located in the middle of trimers appeared between – 91.2 and – 91.3 ppm [21,34].

3.2 Chemical reactions kinetics

We performed kinetics experiments at pH 3.8, 4.1 and 4.4, and at 277.2 K, 283.2 K, 293.2 K and 313.2 K. The evolution of the hydrolyzed species had a common pattern regardless of the experimental conditions. Fig. 2(a) shows an example of the evolution of the relative concentration of TEOS, the hydrolyzed species and the overall of condensation products at pH 4.1 and 293.2 K. Continuous lines were obtained from the mathematical model that will be discussed in the next section. The concentration of TEOS exponentially decayed as the reaction progressed, and was zero after 750 min,

which suggests that the reaction is not reversible and it is not at equilibrium with the hydrolysis products. Considering the stoichiometric excess of water the kinetics for the first hydrolysis step could be fitted as a first order kinetics to TEOS. The four products derived from TEOS hydrolysis presented a relative maximum in their concentration curves. The initial increase in concentration is offset by the hydrolysis reaction of the intermediate products. The maximum relative concentration was at 0.166 for Si $(OC_2H_5)_3(OH)$ and 0.060 for Si $(OC_2H_5)_2(OH)_2$ after 90 min; and at 0.197 for $Si(OC_2H_5)(OH)_3$ and 0.378 for $Si(OH)_4$ after 310 min. The fact that the relative concentrations of $Si(OC_2H_5)_3(OH)$ and $Si(OC_2H_5)_2(OH)_2$ were smaller than the initial relative concentration of TEOS indicates that the second and third hydrolyses were faster than the first one [23]. The shapes of the curves for the species $Si(OC_2H_5)(OH)_3$ and $Si(OH)_4$ were similar. The relative concentration of the later was approximately double the concentration of the former. Indeed, a correlation between $Si(OC_2H_5)(OH)_3$ and $Si(OH)_4$ concentrations was found to have a quadratic regression coefficient of 0.987 through all the experimental runs (see Fig. S1 in Supplementary Material). Condensation species from intermediate hydrolyzed species were not detected. Indeed, condensation species only came from $Si(OH)_4$ and could only be detected when its concentration was approximately 0.10 mol L^{-1}. The relative concentration of the condensed species describe a convex sigmoidal curve up to 310 min and the slope of the curve decreases above 750 min. This curve would mean that the condensation of the fully hydrolyzed $Si(OH)_4$ may be the limiting step of the overall procedure.

Fig. 2(b) presents the fractional yield curves for hydrolyzed and condensed species as a function of the conversion level of TEOS. For TEOS conversion lower than 0.5, $Si(OC_2H_5)_3(OH)$ was the predominant hydrolyzed species whereas for fractional conversions higher than 0.5, the highest concentration corresponded to $Si(OH)_4$. The condensed species appeared for TEOS conversion above 0.5. According to these results, condensation mainly takes place among highly hydrolyzed species and it is unfavorable for less partially hydrolyzed species. This confirms published data by Fyfe and Aroca who reported that $Si(OH)_4$ provides the majority of active hydroxyls and that alcohol producing condensation reaction are negligible for the reaction of TEOS in acidic media with concentration of water above the stoichiometric ratio [10,35]. The plot of relative concentration as a function of TEOS conversion also gives information on the relative

magnitude of the kinetic constants of the reaction. Furthermore, the accumulation of the relative concentration of $Si(OH)_4$ with a maximum at 0.8 TEOS conversion may indicate that the condensation of $Si(OH)_4$ to form ≡Si−O−Si≡ is the limiting step (Eq. (5)). For every value of pH and temperature, the concentration of $Si(OH)_4$ is approximately double that of $Si(OC_2H_5)(OH)_3$ in the range 0.4 – 0.95 (Fig. S1), which is characteristic of reactions at equilibrium. For the sake of brevity, we will pay attention to the evolution of $Si(OH)_4$ and the initial stages of condensation. The evolution of rest of hydrolyzed species are included in the Supplementary Material file (see Figs. S2 to S4).

Fig. 3 (a), (c) and (e) shows the relative concentration of $Si(OH)_4$ as a function of time at 277.2 K, 283.2 K, 293.2 K and 313.2 K and pH 3.8, 4.1 and 4.4. The curves are typical of consecutive reactions. The concentration of $Si(OH)_4$, which is the product of the hydrolysis of $Si(OC_2H_5)(OH)_3$, increased rapidly to a maximum and then it decayed at a much slower rate due to the condensation reactions to form siloxane bonds. For each pH, the relative maxima on the curves shifted to lower reaction times as the temperature increased from 277.2 to 313.2 K, which means that both hydrolysis and condensation rate speeded up with temperature. The maxima for the relative concentration is around 0.40, which corresponds to ~0.17 mol L^{-1} $Si(OH)_4$ and marks the beginning of condensation. The rate of the exponential decrease of fully hydrolyzed species was more pronounced when pH went down from 4.4 to 3.8.

The variation of the relative concentration of $Si(OH)_4$ as a function of TEOS conversion is plotted in Fig. 3 (b), (d) and (f). In all experimental investigated conditions, the shape of the curves was similar. For TEOS conversion up to ~0.20, the relative concentration was negligible, which indicates that hydrolyzed TEOS is distributed between $Si(OC_2H_5)_3(OH)$, $Si(OC_2H_5)_2(OH)_2$, and $Si(OC_2H_5)(OH)_3$. The concentration of $Si(OH)_4$ built up for TEOS conversion between 0.2 and 0.7, reached a maximum at approximately 0.9 and steeply decreased for conversion degrees higher than 0.9. The curves for different experimental conditions overlapped, therefore, although the reaction rate increased with the temperature and the concentration of oxonium ions, the relative concentration of $Si(OH)_4$ only depends on the TEOS fractional conversion, which suggests a common reaction pathway and that the reaction mechanisms are similar in the studied temperature range of 277.2 K – 313.2 K.

Fig. 4 (a), (c) and (e) shows the kinetic curves for the variation of the relative concentration of the overall condensed species at the studied conditions. The curves present a sigmoid shape with an induction period, an increase in the relative concentration of condensed species, and a stabilization of the relative concentration. In a similar way as for $Si(OH)_4$, the curves shifted to lower times with increasing temperature and oxonium ion concentration. For each temperature, the reaction rate increased when pH decreased from 4.4 to 3.8. The relative concentration of condensed species as a function of TEOS conversion is shown in Fig. 4 (b), (d) and (f). These curves can be described by an induction TEOS conversion of up to 0.60, where relative concentration was no detected, so ruling out a direct participation of TEOS directly in the condensation reaction giving off ethanol. Differences in pH or temperature are not significant; therefore, reaction mechanisms must be similar.

3.3 Mathematical model analysis

The model assumes that the concentration of $Si(OH)_4$ is controlled by the reversible hydrolysis of $Si(OC_2H_5)(OH)_3$, the first condensation step of the $Si(OH)_4$ monomer to form a dimer, and the condensation reaction between $Si(OH)_4$ and condensed species. According to the model (Eqs. (5) and (6)), fully hydrolyzed species react to form dimers (k_{c1}) which, in turn, may react with $Si(OH)_4$ monomers to form larger chains (k_{c2}). Under the reaction conditions, $Si(OH)_4$ presents the most active hydroxyls giving rise to condensation products; indeed, other condensation products are not observed when $Si(OH)_4$ is not present in the reaction mixture.

These results confirm published data for TEOS hydrolysis and condensation reactions where reactions producing ethanol were negligible [10,35]. The experimental data from each reaction at different combinations of pH and temperature were used to estimate the kinetic parameters of the hydrolysis and condensation reactions, which are presented in Table 1. The table includes the four constants for the hydrolysis reactions from TEOS to $Si(OH)_4$, two condensation constants to form siloxane bonds from $Si(OH)_4$, and the equilibrium constant for the fourth hydrolysis reaction that was considered as reversible. These parameters were determined by direct search (Section 2.3). The constants for the hydrolysis of TEOS and $Si(OC_2H_5)_3(OH)$ were also determined by the

Levenberg-Marquardt method using 8.53 mol L^{-1} as the initial concentration of water, which was considered constant during the hydrolysis. In general, the differences in the value of the constants determined by the direct search and Levenberg-Marquardt method were lower than ±10%.

The hydrolysis kinetic constants increased in each step, $k_{h1} < k_{h2} < k_{h3} < k_{h4}$, in all the studied reaction conditions, which follows the same incremental trend reported by several authors, although the constants were higher than published data [9-11,36,37]. Nevertheless, this discrepancy can be explained by the difference in the experimental conditions. For example, Fyfe and Aroca reported kinetic constants for pH values between 2.33 and 3.35 for acidified water with HCl, whereas in our experiments, we adjusted the pH of the initial mixture of TEOS, ethanol and water. Therefore, the actual concentration of oxonium ions was higher in our experiments than in those by Fyfe and Aroca [10].

However, the trend is opposite to other experimental results reported by other authors in which the kinetic constants decrease in magnitude as the hydrolysis reactions advance [2,8].These studies have in common that the initial concentration of water was below the stoichiometric ratio. Consequently, the fact that water is consumed during the first and second hydrolysis reactions to produce $Si(OC_2H_5)_3(OH)$ and $Si(OC_2H_5)_2(OH)_2$ would explain the decreasing trend for the magnitude of the kinetic hydrolysis constants as the reaction progresses. Depla et al. investigated the initial oligomerization reaction pathways in acid-catalyzed silica sol-gel reactions under substoichiometric water:TEOS molar ratio ($0.2 \leq r \leq 1.2$) and showed that "The molar ratio had a strong influence on the reaction kinetics" [12].

The condensation reaction rate for dimer formation is lower than that for the formation of the fully hydrolyzed $Si(OH)_4$, which is confirmed by the buildup of the concentration of this species (Fig. 2). The accumulation of $Si(OH)_4$ also affects the concentration of $Si(OC_2H_5)(OH)_3$ (Eq. 4) because, according to the experimental results, these species are at equilibrium (k_{eq} (k_{h4}/k_{-h4})). The magnitude of the equilibrium constants deduced from the different temperature and pH values is consistent with the experimental results. The ratio of $Si(OH)_4$ to $Si(OC_2H_5)_3(OH)$ concentration is 2.08.

$$K_{eq\ (K_{h4}/K_{-h4})}=\frac{[Si(OH)_4][C_2H_5OH]}{[Si(OC_2H_5)(OH)_3][H_2O]}\sim 2.08\frac{[C_2H_5OH]}{[H_2O]} \quad (11)$$

For an initial concentration of TEOS 0.426 mol L^{-1}, at equilibrium the moles of ethanol will be around 14 and the moles of water around 7, which accounts for an etanol:water ratio of 2 and an equilibrium constant of slightly more than 4, in agreement with the equilibrium constant deduced by the model.

The temperature dependence of rate constants can be represented by the Arrhenius equation. The standard method for obtaining the activation energy, E_a, is to plot the experimental rate constant data at different temperatures on an Arrhenius plot for each pH setting a reference temperature:

$$\ln k_i(T)= \ln k_i(298.2)-\frac{E_{a,i}}{R}\left(\frac{1}{T}-\frac{1}{298.2}\right) \quad (12)$$

where $k_i(T)$ is the kinetic constant of a species i at a given absolute temperature, $k_i(298.2)$ is the estimated kinetic constant at 298.2 K, and T is the absolute temperature. The slope gives $-E_a/R$, where R is 8.3145 J mol^{-1} K^{-1} and the origin ordinate is the Neperian logarithm of the kinetic constant. Fig. 5 shows the plot of the kinetic constants at 298.2 K as a function of the concentration of oxonium ions. The kinetic constants for the hydrolysis and condensation reactions increased linearly with the concentration of H_3O^+, therefore the slope of the plots provides the catalyst independent rate constants for individual reactions. The magnitude of the rate constants increases with the number of hydroxyls of the silicon species, which agrees with published data [10,36,37]. The kinetic constants for the formation of dimers from $Si(OH)_4$ and the polymerization of dimers with $Si(OH)_4$ were lower than the hydrolysis constants, proving that in acidic media condensation is the rate limiting step.

The fact that the kinetic constants are linearly related to the oxonium ion concentration indicates that the mechanisms for the catalysis is similar for these reactions and that a model can be formulated in which pH-independent rate constants, k_i^T, can be described as a function of the Arrhenius equation presented before.

$$k_i'(T) = k_i \quad (T) \cdot [H_3O^+] \qquad (13)$$

Therefore, the system can be described according to thirteen parameters, six of them corresponding to the kinetic constants at 298.2 K, six to the activation energies, and one to the equilibrium constant for the fourth hydrolysis which has been shown to be constant in the range of experimental temperature. Table 2 includes the estimated parameters using the experimental data obtained from the ^{29}Si NMR chemical shifts. Figures 2-5 already include the predictions from the mathematical model including the thirteen parameters. In general, the calculated curves fit the experimental data.

4 Discussion

The hydrolysis rate seems to be governed by the attack of the oxonium to the ethoxy group, as it is evidenced by the linear relation between the kinetic constants for hydrolysis and condensation reactions and the oxonium concentration (Fig. 5). Protonation of alkoxy groups withdraws electron density from silicon, making it more electrophilic which, in turn, favors the nucleophilic attack of water that according to the literature is assumed to be bimolecular. Furthermore, the protonated ethoxy group is a better leaving group than deprotonated ethoxy group. The water molecules attacks from the opposite side to the protonated ethoxy groups and acquires a partial positive charge. The transition state decays by displacement of alcohol accompanied by inversion of the configuration on silicon tetrahedron [2].

Under the reaction conditions, the pH-independent rate constants increased as the hydrolysis went forward, and the kinetic constant for the formation of $Si(OH)_4$ was approximately 45 times higher than the constant for the first hydrolysis step from TEOS (Table 2). The pH-independent rate constant for condensation between $Si(OH)_4$ was 156 $L^2\ mol^{-2}\ min^{-2}$, around four times lower than the last hydrolysis constant, but near 20 times higher than the constant for the condensation between condensed species and $Si(OH)_4$.

Steric factors exert noticeable effect on the hydrolytic stability of alkoxysilanes and related precursors [2]. Alkyl substituents with longer chain and bulkier alkoxy groups retard the hydrolysis of alkoxysilanes [38]. Bulkier ethoxy groups hinder the

electrophilic attack by water molecules more than hydroxyl groups, therefore, hydrolysis must be faster when OH groups replace ethoxy groups. Steric hindrance slows down the kinetics in at least two steps of the reaction mechanism by obstructing (a) the electrophilic attack of oxonium ion to the ethoxy group, and (b) the nucleophilic attack of water to silicon atom to form the pentacoordinate intermedium. Besides steric factors, effects, both the electrophilic attack of oxonium ions to ethoxy groups and the nucleophilic attack of water to silicon should be favored by the higher ability of hydrolyzed species to form hydrogen bonds with oxonium and water. The higher mobility of more hydrolyzed species in the reaction medium may also increase the pH-independent kinetic constants.

The activation energies for the hydrolysis reactions are characteristic for reactions that progress under mild temperatures. Although we did not find significant differences in the activation energies for the hydrolysis steps, the mathematical model indicates a steady increase from 34.5 kJ mol^{-1} for the first hydrolysis to 39.2 kJ mol^{-1} in the last step, which confirms that these last hydrolysis steps are favored by an increase in the temperature. The activation energy for the condensation reaction from $Si(OH)_4$ was ca. 10 kJ mol^{-1} higher than the largest activation energy in hydrolytic reactions. Chemical shift of the silicon monomeric species can give some insight as it provides information about the net charge on the silicon atom because the relative screening constant for ^{29}Si is linearly correlated to the net charge on the silicon atom between -40 ppm and -120 ppm chemical shift range [39]. In that range, increasing the net positive charge induces a shielding and leads to high-field shift. The hydrolyzed species appeared at lower field when compared to TEOS signal. On the other hand, the first condensed species appeared at around -82 ppm, almost like TEOS. These results evidence that the replacement of an OR group by a hydroxyl one during the hydrolysis corresponds to a decrease in the net positive charge on the silicon atom [33,34], which has been attributed to a weakening of the effective oxygen inductive effect in the more ionic hydroxyl bond [40]. Therefore, the net positive charge on the silicon atom is as follows: $Si(OC_2H_5)_4 > Si(OC_2H_5)_3(OH) > Si(OC_2H_5)_2(OH)_2 > Si(OC_2H_5)(OH)_3 > Si(OH)_4$. (Fig. 1) [33,39]. These decrease in net positive charge on silicon promotes the protonation of the ethoxy group, increases the distance of Si-O bond, and makes ethanol a better leaving group. The inductive effect, magnetic shielding tensors and charges on

silicon atom for TEOS and hydrolyzed species have been estimated by Quantum Mechanics (Table 3). Protonation of the ethoxy occurs through a very low energy transition state and is assumed to be very fast, being the nucleophilic attack of water to silicon *via* a pentacoordinate intermedium the rate limiting step [41]. The observed trend for the activation energy values can be related to the slight decrease on the net positive charge of the silicon atoms as the hydrolysis progresses as it is shown by QM calculations.

The used reaction conditions with a large excess of H_2O not only allowed estimating kinetic constant and activation energies for the hydrolysis of TEOS but also for the first condensation step of $Si(OH)_4$ as well as for the condensation of $Si(OH)_4$ with other condensed species. Although these estimation is less reliable, the kinetic constant for the dimerization from $Si(OH)_4$ is approximately 20 times higher than the kinetic constant for the reaction of this monomer with the condensed species, which may be justified by the lower mobility of condensed species and lower accessibility of silanol groups in these species. Activation energies (ca. 50 $kJ \cdot mol^{-1}$), for both condensation reactions were approximately 10 kJ mol^{-1} higher than those for hydrolysis that makes condensation the rate limiting step for the gelling process. This is in agreement with the equilibrium that was found between $Si(C_2H_5O)(OH)_3$ and $Si(OH)_4$, that is the only reversible hydrolysis reaction that could be found under our reaction conditions.

Conclusions

We studied the kinetics of TEOS between pH 3.8 and 4.4, and four temperature values in the range 277.2 – 313.2 K, with a TEOS:ethanol:water molar ratio 1:30:20, respectively. In these experimental conditions, the evolution of hydrolyzed and condensed species had a common pattern. Both hydrolysis and condensation rate speeded up with temperature. The variation of the relative concentration of the hydrolyzed species as a function of TEOS conversion overlapped, which denotes a common reaction pathway. The kinetic constants for hydrolysis reactions increased in each step $k_{h1} < k_{h2} < k_{h3} < k_{h4}$, but the condensation rate was lower for dimer formation than for the formation of the fully hydrolyzed $Si(OH)_4$.

The system was described according to thirteen parameters: six of them for the kinetic constants estimated at 298.2 K, six to the activation energies, and one to the equilibrium constant for the fourth hydrolysis. The pH-independent rate constants increased as the hydrolysis went forward. The mathematical model shows a steady increase in the activation energy from 34.5 kJ mol^{-1} for the first hydrolysis to 39.2 kJ mol^{-1} in the last step. The activation energy for condensation reaction from $Si(OH)_4$ was ca. 10 kJ mol^{-1} higher than the largest activation energy in the hydrolytic reactions. The electrophilic attack of the oxonium ion to the ethoxy group seems to govern the hydrolysis rate.

Acknowlegments

This work was supported by "Ministerio de Economía, Industria y Competitividad" (MAT2016-78155-C2-2-R). Paula Moriones is thankful to the "Departamento de Industria y Tecnología, Comercio y Trabajo" of Navarre Government for a fellowship.

Compliance with ethical standards

Conflict of interest: The authors declare that they have no conflict of interest.

References

1. Sanchez C, Belleville P, Popall M, Nicole L (2011) Applications of advanced hybrid organic-inorganic nanomaterials: from laboratory to market. Chemical Society Reviews 40 (2):696-753. doi:10.1039/C0cs00136h

2. Brinker CJ, Scherer GW (1990) Sol-Gel Science: The Physics and Chemistry of Sol-Gel Processing. Academic Press, New York, USA

3. Pierre AC (1998) Introduction to Sol-Gel Processing. Kluwer, Boston, USA

4. Wright JD, Sommerdijk NAJM (2001) Sol-Gel Materials: Chemistry and Applications, vol 4. Advanced Chemistry Texts. Taylor & Francis, London, UK

5. Estella J, Echeverria JC, Laguna M, Garrido JJ (2007) Silica xerogels of tailored porosity as support matrix for optical chemical sensors. Simultaneous effect of pH, ethanol : TEOS and water : TEOS molar ratios, and synthesis temperature on gelation

time, and textural and structural properties. Journal of Non-Crystalline Solids 353 (3):286-294. doi:10.1016/j.jnoncrysol.2006.12.006

6. Estella J, Echeverria JC, Laguna M, Garrido JJ (2007) Effects of aging and drying conditions on the structural and textural properties of silica gels. Microporous and Mesoporous Materials 102 (1-3):274-282. doi:10.1016/j.micromeso.2007.01.007

7. Estella J, Echeverria JC, Laguna M, Garrido JJ (2008) Effect of supercritical drying conditions in ethanol on the structural and textural properties of silica aerogels. Journal of Porous Materials 15 (6):705-713. doi:10.1007/s10934-007-9156-9

8. Jitianu A, Britchi A, Deleanu C, Badescu V, Zaharescu M (2003) Comparative study of the sol-gel processes starting with different substituted Si-alkoxides. Journal of Non-Crystalline Solids 319 (3):263-279. doi:10.1016/S0022-3093(03)00007-3

9. Pouxviel JC, Boilot JP (1987) Kinetic Simulations and Mechanisms of the Sol-Gel Polymerization. Journal of Non-Crystalline Solids 94 (3):374-386. doi:10.1016/S0022-3093(87)80072-8

10. Fyfe CA, Aroca PP (1995) Quantitative Kinetic-Analysis by High-Resolution Si-29 Nmr-Spectroscopy of the Initial-Stages in the Sol-Gel Formation of Silica-Gel from Tetraethoxysilane. Chemistry of Materials 7 (10):1800-1806. doi:10.1021/Cm00058a008

11. Sanchez J, McCormick A (1992) Kinetic and thermodynamic study of the hydrolysis of silicon alkoxides in acidic alcohol solutions. Journal of Physical Chemistry 96 (22):8973-8979. doi:10.1021/j100201a051

12. Depla A, Lesthaeghe D, van Erp TS, Aerts A, Houthoofd K, Fan F, Li C, Van Speybroeck V, Waroquier M, Kirschhock CEA, Martens JA (2011) Si-29 NMR and UV-Raman Investigation of Initial Oligomerization Reaction Pathways in Acid-Catalyzed Silica Sol-Gel Chemistry. Journal of Physical Chemistry C 115 (9):3562-3571. doi:10.1021/jp109901v

13. Pouxviel JC, Boilot JP, Beloeil JC, Lallemand JY (1987) Nmr-Study of the Sol-Gel Polymerization. Journal of Non-Crystalline Solids 89 (3):345-360. doi:10.1016/S0022-3093(87)80277-6

14. Zhai Q, Zhou C, Zhao S, Peng C, Han Y (2014) Kinetic Study of Alkoxysilane Hydrolysis under Acidic Conditions by Fourier Transform Near Infrared Spectroscopy Combined with Partial Least-Squares Model. Industrial & Engineering Chemistry Research 53 (35):13598-13609. doi:10.1021/ie5012195

15. Gualandris V, Babonneau F, Janicke MT, Chmelka B (1998) NMR studies on hydrolysis and condensation reactions of alkoxysilanes containing Si-H bonds. Journal of Sol-Gel Science and Technology 13 (1-3):75-80. doi:10.1023/A:1008651221693

16. Babonneau F, Maquet J (2000) Nuclear magnetic resonance techniques for the structural characterization of siloxane-oxide hybrid materials. Polyhedron 19 (3):315-322. doi:10.1016/s0277-5387(99)00361-7

17. Tejedor-Tejedor MI, Paredes L, Anderson MA (1998) Evaluation of ATR-FTIR spectroscopy as an "in situ" tool for following the hydrolysis and condensation of alkoxysilanes under rich H2O conditions. Chemistry of Materials 10 (11):3410-3421. doi:10.1021/Cm980146l

18. Sanchez J, Rankin SE, McCormick AV (1996) Si-29 NMR kinetic study of tetraethoxysilane and ethyl-substituted ethoxysilane polymerization in acidic conditions. Industrial & Engineering Chemistry Research 35 (1):117-129. doi:10.1021/ie950246q

19. Assink RA, Kay BD (1988) Sol-gel kinetics. 3. Test of the statistical reaction model. Journal of Non-Crystalline Solids 107 (1):35-40. doi:10.1016/0022-3093(88)90089-0

20. Boonstra AH, Bernards TNM (1989) Hydrolysis Condensation-Reactions in the Acid Step of a 2-Step Silica Sol-Gel Process, Investigated with Si-29 Nmr at -75-Degrees-C. Journal of Non-Crystalline Solids 108 (3):249-259. doi:10.1016/0022-3093(89)90295-0

21. Mazur M, Mlynarik V, Valko M, Pelikan P (2000) The time evolution of the sol-gel process: Si-29 NMR study of the hydrolysis and condensation reactions of tetraethoxysilane. Applied Magnetic Resonance 18 (2):187-197. doi:10.1007/Bf03162110

22. Fyfe CA, Aroca PP (1997) A kinetic analysis of the initial stages of the sol-gel reactions of methyltriethoxysilane (MTES) and a mixed MTES/tetraethoxysilane

system by high-resolution Si-29 NMR spectroscopy. Journal of Physical Chemistry B 101 (46):9504-9509. doi:10.1021/jp971559x

23. Houston PL (2001) Chemical Kinetics and Reaction Dynamics. 1st edn. McGraw-Hill, New York, USA

24. Frisch MJ, Trucks GW, Schlegel HB, Scuseria GE, Robb MA, Cheeseman JR, Scalmani G, Barone V, Mennucci B, Petersson GA, Nakatsuji H, Caricato ML, X. , Hratchian HP, Izmaylov AF, Bloino J, Zheng G, Sonnenberg JL, Hada M, Ehara M, Toyota K, Fukuda R, Hasegawa J, Ishida M, Nakajima T, Honda Y, Kitao O, Nakai H, Vreven T, Montgomery J, J. A. , Peralta JE, Ogliaro F, Bearpark M, Heyd JJ, Brothers E, Kudin KN, Staroverov VN, Keith T, Kobayashi R, Normand J, Raghavachari K, Rendell A, Burant JC, Iyengar SS, Tomasi J, Cossi M, Rega N, Millam JM, Klene M, Knox JE, Cross JB, Bakken V, Adamo C, Jaramillo J, Gomperts R, Stratmann RE, Yazyev O, Austin AJ, Cammi R, Pomelli C, Ochterski JW, Martin RL, Morokuma K, Zakrzewski VG, Voth GA, Salvador P, Dannenberg JJ, Dapprich S, Daniels AD, Farkas O, Foresman JB, Ortiz JV, Cioslowski J, Fox DJ (2010) Gaussian 09. Revision C.01 edn., Wallingford CT, USA

25. Adamo C, Barone V (1998) Exchange functionals with improved long-range behavior and adiabatic connection methods without adjustable parameters: The mPW and mPW1PW models. Journal of Chemical Physics 108 (2):664-675. doi:10.1063/1.475428

26. Cioslowski J (1989) A New Population Analysis Based on Atomic Polar Tensors. Journal of the American Chemical Society 111 (22):8333-8336. doi:10.1021/Ja00204a001

27. Reed AE, Curtiss LA, Weinhold F (1988) Intermolecular Interactions from a Natural Bond Orbital, Donor-Acceptor Viewpoint. Chemical Reviews 88 (6):899-926. doi:10.1021/Cr00088a005

28. Lee CT, Yang WT, Parr RG (1988) Development of the Colle-Salvetti Correlation-Energy Formula into a Functional of the Electron-Density. Physical Review B 37 (2):785-789. doi:10.1103/PhysRevB.37.785

29. Becke AD (1993) Density-Functional Thermochemistry .3. The Role of Exact Exchange. Journal of Chemical Physics 98 (7):5648-5652. doi:10.1063/1.464913

30. Mclean AD, Chandler GS (1980) Contracted Gaussian-Basis Sets for Molecular Calculations .1. 2nd Row Atoms, Z=11-18. Journal of Chemical Physics 72 (10):5639-5648. doi:10.1063/1.438980

31. Wolinski K, Hinton JF, Pulay P (1990) Efficient implementation of the gauge-independent atomic orbital method for NMR chemical shift calculations. Journal of the American Chemical Society 112 (23):8251-8260. doi:10.1021/ja00179a005

32. Cheeseman JR, Trucks GW, Keith TA, Frisch MJ (1996) A comparison of models for calculating nuclear magnetic resonance shielding tensors. Journal of Chemical Physics 104 (14):5497-5509. doi:10.1063/1.471789

33. Hook RJ (1996) A Si-29 NMR study of the sol-gel polymerisation rates of substituted ethoxysilanes. Journal of Non-Crystalline Solids 195 (1-2):1-15. doi:10.1016/0022-3093(95)00508-0

34. Malier L, Devreux F, Chaput F, Boilot JP (1992) Silicon-29 nuclear magnetic resonance of sol-gel transformation in first steps and after gel time. In: Hench LL, West JK (eds) Chemical Processing of Advanced Materials. John Wiley and Sons, Inc, pp 59-67

35. Colby MW, Osaka A, Mackenzie JD (1988) Temperature-Dependence of the Gelation of Silicon Alkoxides. Journal of Non-Crystalline Solids 99 (1):129-139. doi:10.1016/0022-3093(88)90465-6

36. Yang H, Ding Z, Jiang Z, Xiaoping X (1989) Sol-gel process kinetics for Si(OEt)4. Journal of Non-Crystalline Solids 112 (1-3):449-453

37. Chojnowski J, Cypryk M, Kazmierski K, Rozga K (1990) The Reactivity of Monomeric Silanol Intermediates in the Hydrolytic Polycondensation of Tetraethoxysilane in Acidic Media. Journal of Non-Crystalline Solids 125 (1-2):40-49. doi:10.1016/0022-3093(90)90321-C

38. Aelion R, Loebel A, Eirich F (1950) Hydrolysis of Ethyl Silicate. Journal of the American Chemical Society 72 (12):5705-5712. doi:10.1021/Ja01168a090

39. Devreux F, Boilot JP, Chaput F, Lecomte A (1990) Si-29 NMR-Study of Silicon Alkoxides - from the Condensation Kinetics in Solution to the Determination of the Fractal Dimension in Aerogels. In: Brinker CJ, Zelinsky BJ, Ulrich DR, Clark DE (eds) Better Ceramics through Chemistry IV, San Francisco, 1990. Materials Research Society, pp 211-216

40. Devreux F, Boilot JP, Chaput F, Lecomte A (1990) Sol-Gel Condensation of Rapidly Hydrolyzed Silicon Alkoxides - a Joint Si-29 NMR and Small-Angle X-Ray-Scattering Study. Physical Review A 41 (12):6901-6909. doi:10.1103/PhysRevA.41.6901

41. Cheng XL, Chen DR, Liu YJ (2012) Mechanisms of Silicon Alkoxide Hydrolysis-Oligomerization Reactions: A DFT Investigation. Chemphyschem 13 (9):2392-2404. doi:10.1002/cphc.201200115

Figure captions

Fig. 1 (a) Time dependence of the ^{29}Si NMR spectra at pH 4.1 and 293.2 K, (b) Detail of condensed species

Fig. 2 Relative concentrations of TEOS, hydrolyzed species and the total condensed species at pH 4.1 and 293.2 K as a function of (a) reaction time and (b) TEOS conversion. Symbols (■, TEOS; ◇, $Si(OC_2H_5)_3(OH)$; ▼ $Si(OC_2H_5)_2(OH)_2$; × $Si(OC_2H_5)(OH)_3$; ▲, $Si(OH)_4$; ●, total condensed species) show experimental values and continuous lines show the calculated curves

Fig. 3 Relative concentration of $Si(OH)_4$ at 277.2 K (●), 283.2 K (▲), 293.2 K (◆), and 313.2 K (■) as a function of time (a, c and e) and TEOS conversion (b, d and f), measured at pH 3.8, 4.1 and 4.4. Continuous lines show the calculated curves

Fig. 4 Relative concentration of condensed species at 277.2 K (●), 283.2 K (▲), 293.2 K (◆), and 313.2 K (■) as a function of time (a, c and e) and TEOS conversion (b, d and f), measured at pH 3.8, 4.1 and 4.4. Continuous lines show the calculated curves

Fig. 5 Plots of the kinetic constants at 298.2 K, as a function of the concentration of oxonium ions: (a) hydrolysis kinetic rate constants and (b) condensation kinetic rate constants. Legend: ■, k'_{h1}; ●, k'_{h2}; ▲, k'_{h3}; ▼, k'_{h4}; ◇, k'_{c1}; ▽, k'_{c2}

Figures

Fig. 1

(a) (b)

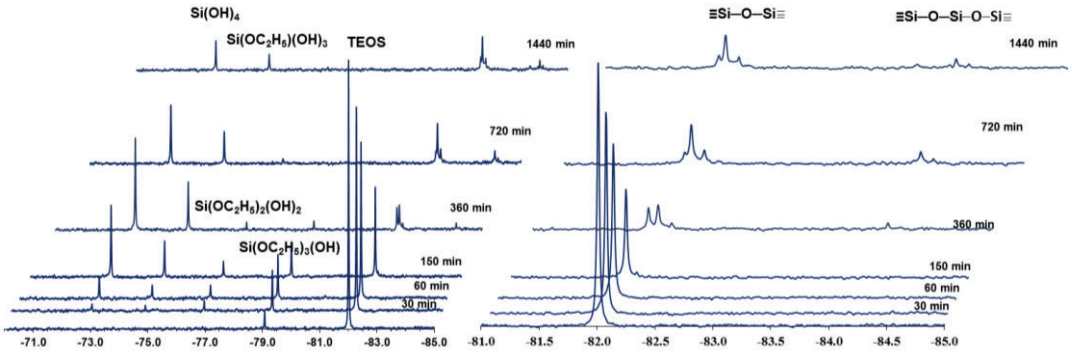

Fig. 2

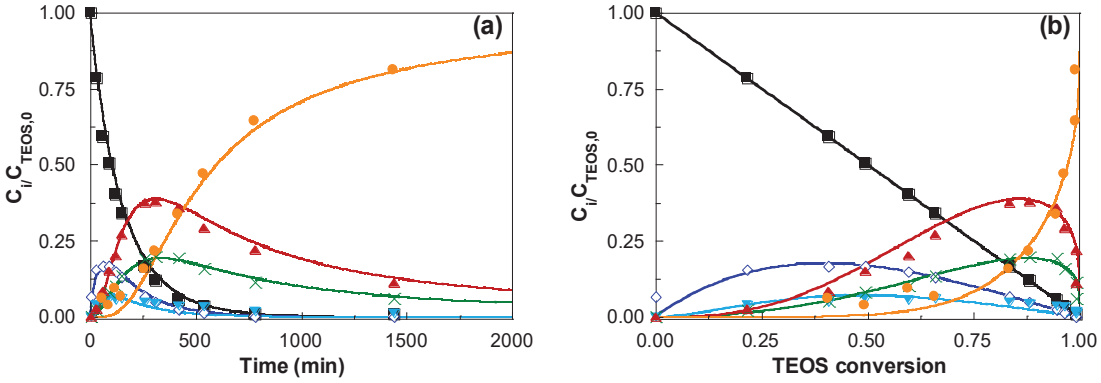
(a)
1.00
0.75
0.50
0.25
0.00
$C_i/C_{TEOS,0}$
0
500
1000
1500
2000
Time (min)
(b)
1.00
0.75
0.50
0.25
0.00
$C_i/C_{TEOS,0}$
0.00
0.25
0.50
0.75
1.00
TEOS conversion

Fig. 3

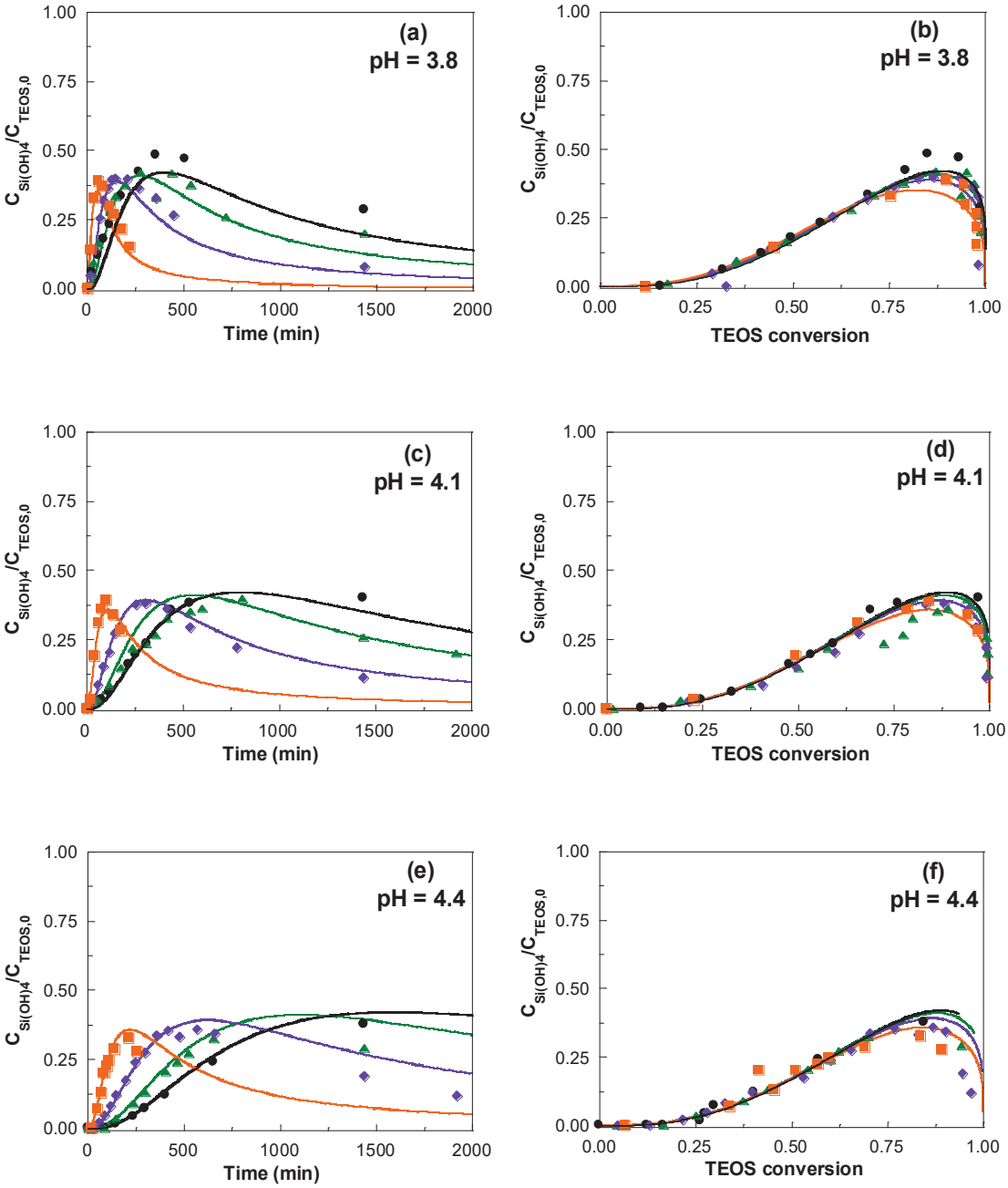
(a)
pH = 3.8
(b)
pH = 3.8
(c)
pH = 4.1
(d)
pH = 4.1
(e)
pH = 4.4
(f)
pH = 4.4
$C_{Si(OH)4}/C_{TEOS,0}$
Time (min)
TEOS conversion
0.00
0.25
0.50
0.75
1.00
0
500
1000
1500
2000

Fig. 4

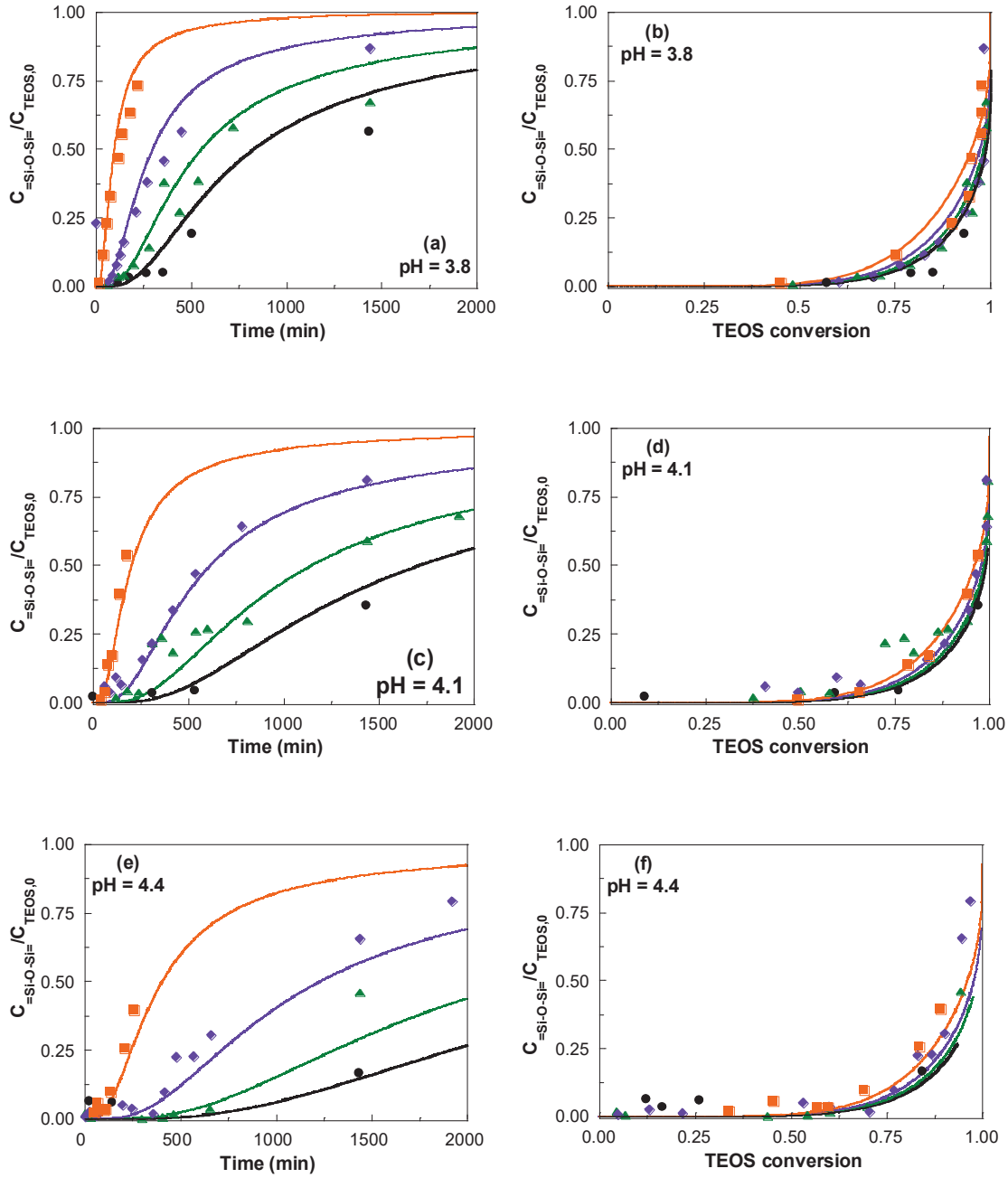
(a)
pH = 3.8
(b)
pH = 3.8
(c)
pH = 4.1
(d)
pH = 4.1
(e)
pH = 4.4
(f)
pH = 4.4
Time (min)
TEOS conversion
C=Si-O-Si=/CTEOS,0

Fig. 5

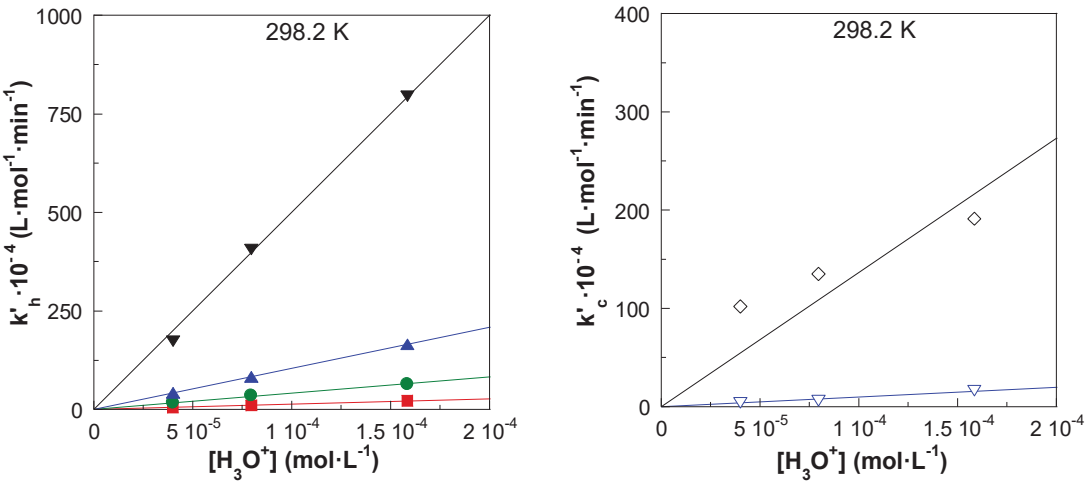
298.2 K
$k'_h \cdot 10^{-4}$ (L·mol^{-1}·min^{-1})
[H_3O^+] (mol·L^{-1})
0
250
500
750
1000
5 10^{-5}
1 10^{-4}
1.5 10^{-4}
2 10^{-4}
298.2 K
$k'_c \cdot 10^{-4}$ (L·mol^{-1}·min^{-1})
[H_3O^+] (mol·L^{-1})
0
100
200
300
400
5 10^{-5}
1 10^{-4}
1.5 10^{-4}
2 10^{-4}

Click here to download Table
Tbl_Moriones_TEOS_kinetics_29Si_NMR.docx

Table 1

Kinetic and equilibrium constants determined for the TEOS hydrolysis-condensation process at the studied parameters: pHs (3.8, 4.1 and 4.4) and temperatures (277.2, 283.2, 293.2 and 313.2 K).

pH	T / K	Kinetic constants for TEOS /10^{-4}·L mol^{-1} min^{-1}								
		k_{h1}		k_{h2}		k_{h3}	k_{h4}	k_{c1}	k_{c2}	K_{eq} (h4/-h4)
		Direct search	Levenberg-Marquardt	Direct search	Levenberg-Marquardt	Direct search	Direct search	Direct search	Direct search	Direct search
3.8	277.2	8.6	8.3	23.9	23.5	72.6	387	35.3	0.6	4.1
	283.2	10.5	10.3	30.3	30.3	97.5	395	74.8	8.3	4.1
	293.2	16.9	16.0	49.4	49.9	122.0	728	140.0	14.0	4.1
	313.2	39.5	37.8	125.0	136.9	293.0	1290	487.0	27.8	4.1
4.1	277.2	3.5	3.3	10.3	9.5	26.5	81.2	20.2	1.8	4.1
	283.2	4.5	4.4	13.2	13.8	28.7	117	52.1	2.3	4.0
	293.2	8.8	8.5	28.3	28.5	62.1	367	110.0	7.5	4.1
	313.2	21.5	19.9	78.9	72.8	193.0	1000	341.0	11.3	4.1
4.4	277.2	1.6	1.5	4.6	4.2	13.2	39.2	21.0	1.8	4.0
	283.2	2.3	2.2	7.4	6.8	18.1	85.8	49.6	3.8	4.1
	293.2	4.3	4.1	14.2	13.6	32.1	87.7	72.1	3.3	4.0
	313.2	9.6	9.2	35.8	33.8	88.5	485.0	241.0	7.2	4.0

Table 2

Kinetic constant ($k_i^{298.2}$) for the TEOS hydrolysis-condensation process and activation energies.

	$k_i^{298.2}$ ($L^2\ mol^{-2}\ min^{-1}$)	E_a ($kJ\ mol^{-1}$)	K (k_{h4}/k_{-h4})
Hydrolysis			
$Si(OC_2H_5)_4 + H_2O \xrightarrow{k_{h1},[H_3O^+]} Si(OC_2H_5)_3(OH) + C_2H_5OH$	12.7 ± 0.1	34.5 ± 0.1	*
$Si(OC_2H_5)_3(OH) + H_2O \xrightarrow{k_{h2},[H_3O^+]} Si(OC_2H_5)_2(OH)_2 + C_2H_5OH$	45.0 ± 0.5	37.2 ± 0.2	*
$Si(OC_2H_5)_2(OH)_2 + H_2O \xrightarrow{k_{h3},[H_3O^+]} Si(OC_2H_5)(OH)_3 + C_2H_5OH$	107 ± 3	38.2 ± 0.3	*
$Si(OC_2H_5)(OH)_3 + H_2O \underset{k_{-h4},[H_3O^+]}{\overset{k_{h4},[H_3O^+]}{\rightleftharpoons}} Si(OH)_4 + C_2H_5OH$	601 ± 20	39.2 ± 0.2	4.0 ± 0.1
Condensation			
$2\ Si(OH)_4 \xrightarrow{k_{c1},[H_3O^+]} (OH)_3Si\text{-}O\text{-}Si(OH)_3 + H_2O$	156 ± 3	49.3 ± 0.2	*
$(OH)(Si(OR)_2O)_n\text{-}Si(OH)_3 + Si(OH)_4 \xrightarrow{k_{c2},[H_3O^+]} (OH)(Si(OR)_2O)_{n+1}\text{-}Si(OH)_3 + H_2O$	8.1 ± 0.9	51.3 ± 0.4	*

*Non-detected

Table 3

Natural and APT (Atomic Polar Tensors) charges, inductive effect and magnetic shielding tensors on Si atom for TEOS and hydrolyzed species.

Compound	Natural	APT	Inductive effect	Magnetic shielding tensor
$Si(OC_2H_5)_4$	2.470	2.478	1.08	419.2
$Si(OC_2H_5)_3(OH)$	2.445	2.395	1.03	412.6
$Si(OC_2H_5)_2(OH)_2$	2.413	2.316	0.98	408.5
$Si(OC_2H_5)(OH)_3$	2.390	2.245	0.93	402.5
$Si(OH)_4$	2.368	2.180	0.88	396.9

* mPW1PW91/6-31G(d) was used for the calculation of the geometries in gas phase, APT and Natural charges (electron population) were estimated using B3LYP/6-311+G(2d,p).

Supplementary Material

Kinetic model formulation (section 2.3)

$$\frac{dC_{Si(OC_2H_5)_4}}{dt} = -k'_{h1} \cdot C_{Si(OC_2H_5)_4} \cdot C_{H_2O} \quad \text{Eq.S1}$$

$$\frac{dC_{Si(OC_2H_5)_3(OH)}}{dt} = k'_{h1} \cdot C_{Si(OC_2H_5)_4} \cdot C_{H_2O} - k'_{h2} \cdot C_{Si(OC_2H_5)_3(OH)} \cdot C_{H_2O} \quad \text{Eq.S2}$$

$$\frac{dC_{Si(OC_2H_5)_2(OH)_2}}{dt} = k'_{h2} \cdot C_{Si(OC_2H_5)_3(OH)} \cdot C_{H_2O} - k'_{h3} \cdot C_{Si(OC_2H_5)_2(OH)_2} \cdot C_{H_2O} \quad \text{Eq.S3}$$

$$\frac{dC_{Si(OC_2H_5)(OH)_3}}{dt} = k'_{h3} \cdot C_{Si(OC_2H_5)_2(OH)_2} \cdot C_{H_2O} - k'_{h4} \cdot C_{Si(OC_2H_5)(OH)_3} \cdot C_{H_2O} + \frac{k'_{h4}}{K_{eq}} C_{Si(OH)_4} \cdot C_{C_2H_5OH} \quad \text{Eq.S4}$$

$$\frac{dC_{Si(OH)_4}}{dt} = k'_{h4} \cdot C_{Si(OC_2H_5)(OH)_3} \cdot C_{H_2O} - \frac{k'_{h4}}{K_{eq}} C_{Si(OH)_4} \cdot C_{C_2H_5OH} - 2 \cdot k'_{c1} \cdot \left(C_{Si(OH)_4}\right)^2 - k'_{c2} \cdot C_{Si(OH)_4} \cdot C_{(OH)(Si(OR)_2O)_n\text{-}Si(OH)_3} \quad \text{Eq.S5}$$

$$\frac{dC_{H_2O}}{dt} = -\left(k'_{h1} \cdot C_{Si(OC_2H_5)_4} + k'_{h2} \cdot C_{Si(OC_2H_5)_3(OH)} + k'_{h3} \cdot C_{Si(OC_2H_5)_2(OH)_2} + k'_{h4} \cdot C_{Si(OC_2H_5)(OH)_3}\right) \cdot C_{H_2O} + \frac{k'_{h4}}{K_{eq}} C_{Si(OH)_4} \cdot C_{C_2H_5OH} + k'_{c1} \cdot \left(C_{Si(OH)_4}\right)^2 + k'_{c2} \cdot C_{Si(OH)_4} \cdot C_{(OH)(Si(OR)_2O)_n\text{-}Si(OH)_3} \quad \text{Eq.S6}$$

$$\frac{dC_{C_2H_5OH}}{dt} = \left(k'_{h1} \cdot C_{Si(OC_2H_5)_4} + k'_{h2} \cdot C_{Si(OC_2H_5)_3(OH)} + k'_{h3} \cdot C_{Si(OC_2H_5)_2(OH)_2} + k'_{h4} \cdot C_{Si(OC_2H_5)(OH)_3}\right) \cdot C_{H_2O} - \frac{k'_{h4}}{K_{eq}} C_{Si(OH)_4} \cdot C_{C_2H_5OH} \quad \text{Eq.S7}$$

$$C_{(OH)(Si(OR)_2O)_n\text{-}Si(OH)_3} = \left(C_{Si(OC_2H_5)_4,\ 0} - C_{Si(OC_2H_5)_4}\right) - \sum_{x=0}^{4} C_{Si(OC_2H_5)_{4-x}(OH)_x} \quad \text{Eq.S8}$$

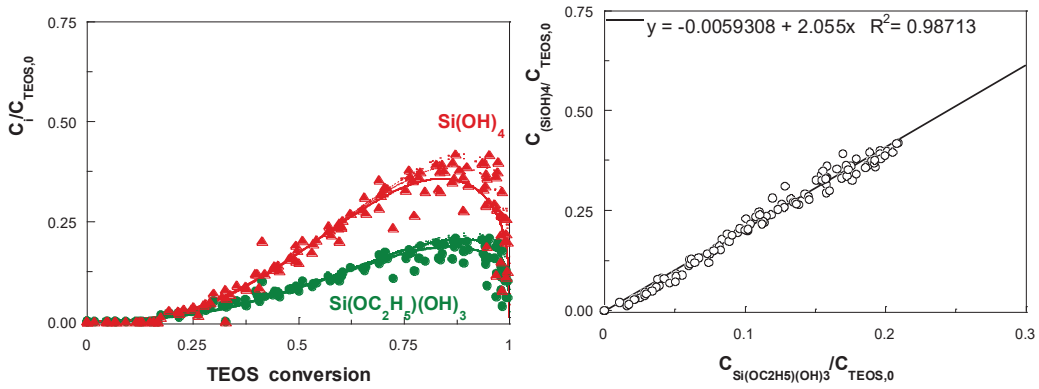

Fig. S1. Relative concentration of $Si(OH)_4$ and $Si(OC_2H_5)(OH)_3$ for the reactions at different pH and temperature.

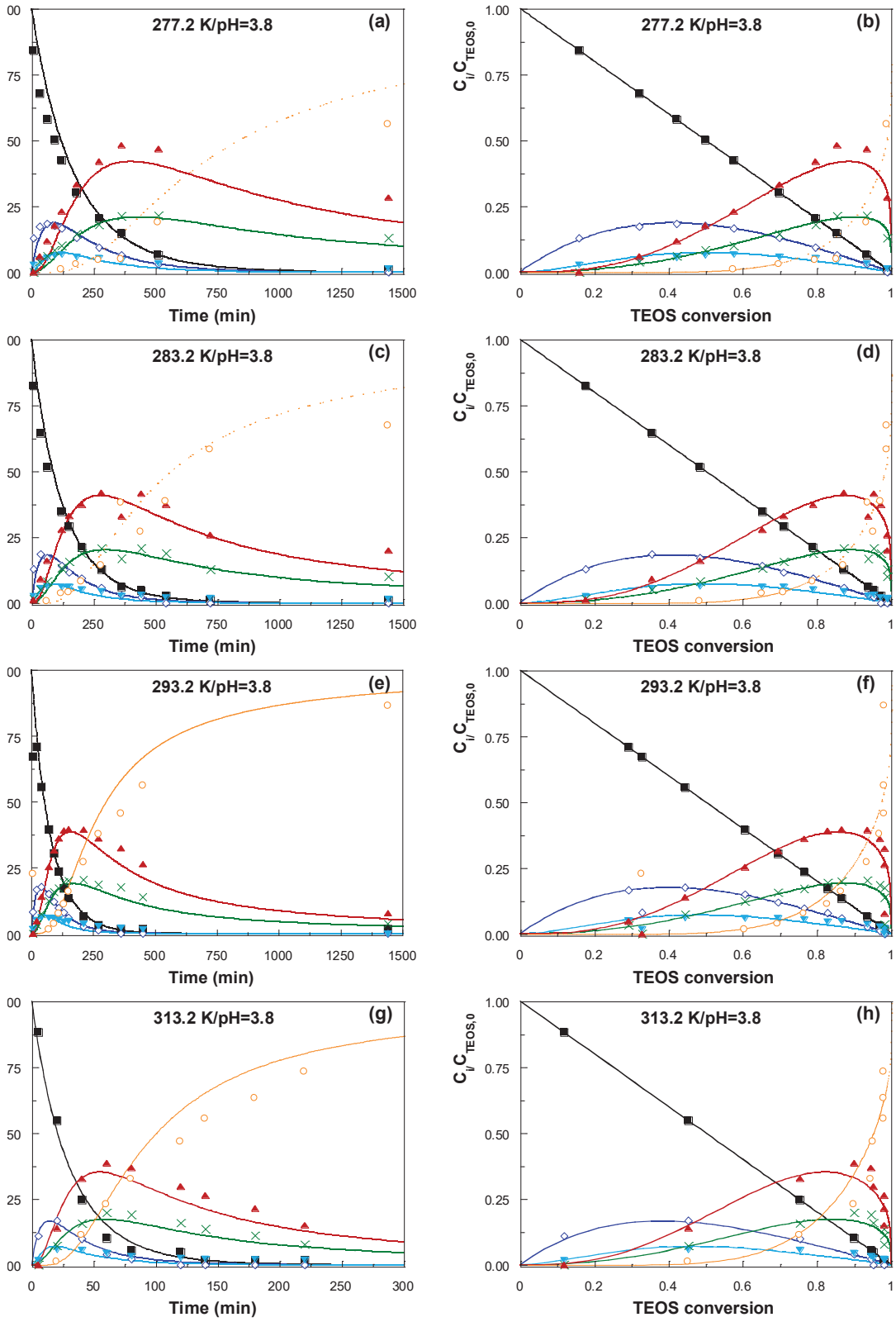

Fig. S2. Relative concentrations of TEOS, hydrolyzed species and the total condensed species at pH 3.8 and 277.2 K, 283.2 K, 293.2 K, and 313.2 K, as a function of (a, c, e, g) reaction time and (b, d, f, h) TEOS conversion. Symbols (■, TEOS; ◇, $Si(OC_2H_5)_3(OH)$; ▼ $Si(OC_2H_5)_2(OH)_2$; ▲, $Si(OC_2H_5)(OH)_3$. × $Si(OH)_4$; ● total condensed species) show experimental values and continuous lines show the calculated curves.

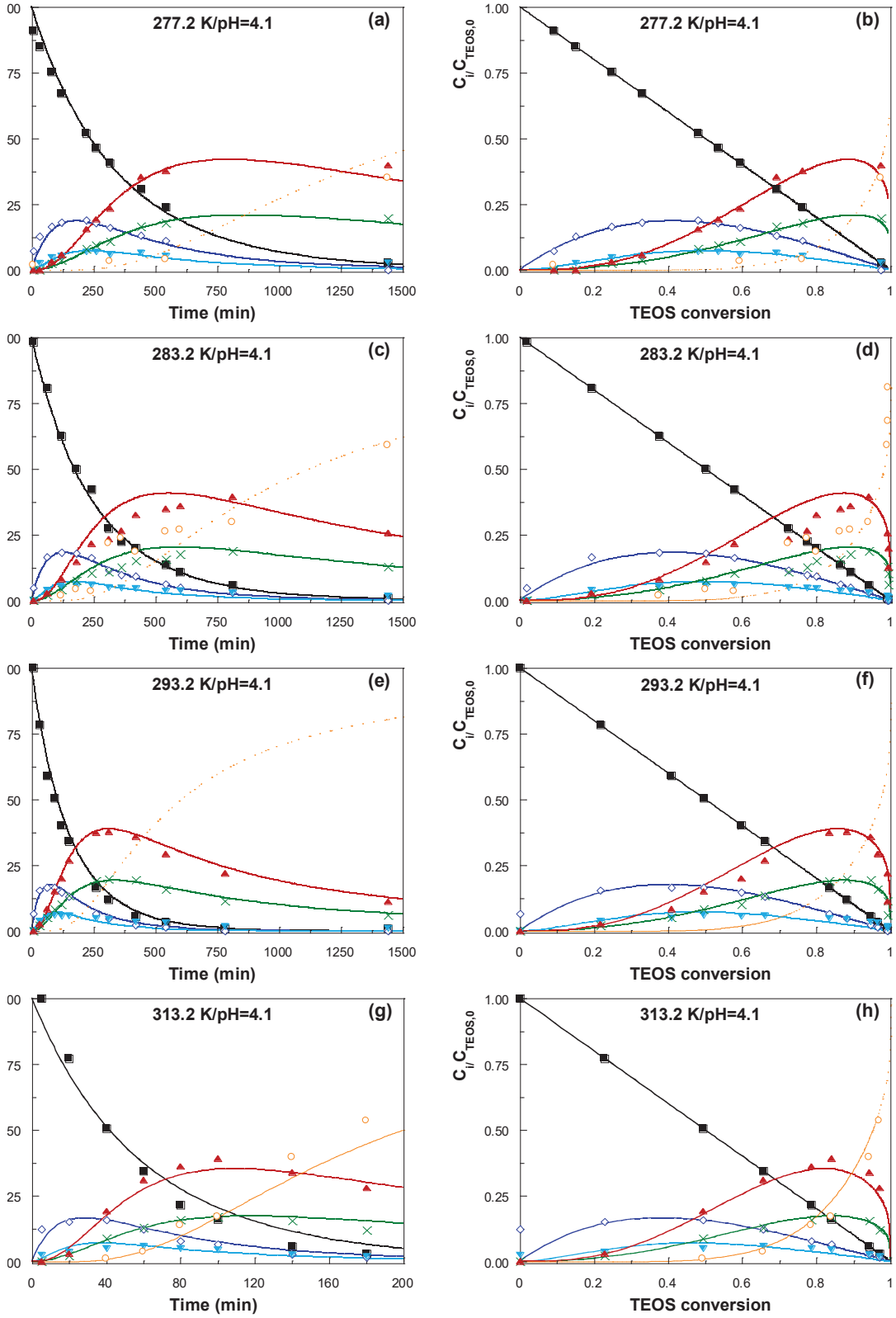

Fig. S3. Relative concentrations of TEOS, hydrolyzed species and the total condensed species at pH 4.1 and at 277.2 K, 283.2 K, 293.2 K and 313.2 K as a function of (a, c, e, g) reaction time and (b, d, f, h) TEOS conversion. Symbols (■, TEOS; ◇, $Si(OC_2H_5)_3(OH)$; ▼ $Si(OC_2H_5)_2(OH)_2$; ▲, $Si(OC_2H_5)(OH)_3$. × $Si(OH)_4$; ● total condensed species) show experimental values and continuous lines show the calculated curves.

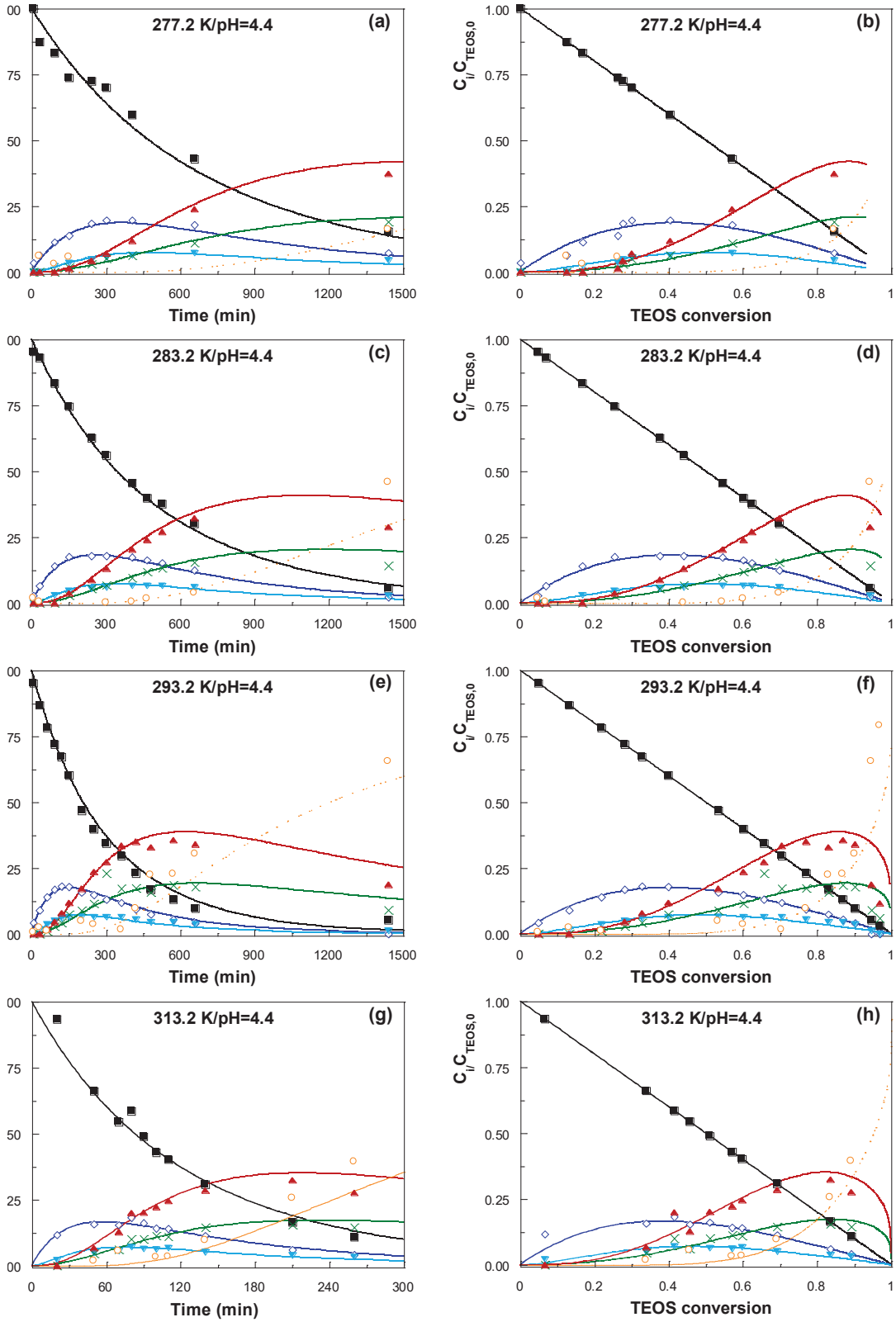

Fig. S4. Relative concentrations of TEOS, hydrolyzed species and the total condensed species at pH 4.4 and at 277.2 K, 283.2 K, 293.2 K and 313.2 K as a function of (a, c, e, g) reaction time and (b, d, f, h) TEOS conversion. Symbols (■, TEOS; ◇, $Si(OC_2H_5)_3(OH)$; ▼ $Si(OC_2H_5)_2(OH)_2$; ▲, $Si(OC_2H_5)(OH)_3$. × $Si(OH)_4$; ● total condensed species) show experimental values and continuous lines show the calculated curves.